

Properties of the Affine Invariant Ensemble Sampler in high dimensions

David Huijser^{*†}Jesse Goodman^{*}Brendon J. Brewer^{*}

December 8, 2024

Abstract

We present theoretical and practical properties of the affine-invariant ensemble sampler Markov chain Monte Carlo method. In high dimensions the affine-invariant ensemble sampler shows unusual and undesirable properties. We demonstrate this with an n -dimensional correlated Gaussian toy problem with a known mean and covariance structure, and analyse the burn-in period. The burn-in period seems to be short, however upon closer inspection we discover the mean and the variance of the target distribution do not match the expected, known values. This problem becomes greater as n increases. We therefore conclude that the affine-invariant ensemble sampler should be used with caution in high dimensional problems. We also present some theoretical results explaining this behaviour.

Key words: Affine Invariant Ensemble Sampler, Markov chain Monte Carlo

1 Introduction

Since the introduction of the Markov chain Monte Carlo methods (MCMC) Metropolis, Rosenbluth, Rosenbluth *et al.* (1953), a large number of different algorithms have been developed, such as Gibbs sampling Geman & Geman (1984), Metropolis-Hastings Hastings (1970), slice sampling Neal (2003) and Hamiltonian MCMC Neal (2011). Each has its own virtues, and its specific properties. A recent innovative MCMC method is the affine-invariant ensemble sampler (AIES) introduced by Goodman & Weare (2009). The intuitive idea behind the AIES (described in Section 2) is compelling. It is also straightforward to implement because its application does not require the user to define a proposal distribution, or add any additional information except the ability to evaluate a function proportional to the density of the target distribution. The structure of the AIES allowed Foreman-Mackey, Hogg, Lang *et al.* (2013) to develop an high quality Python software implementation `emcee`, where the user only needs to define the density of the target distribution. Performance comparisons (for instance Lampart (2012)) show that the AIES is competitive with other common techniques, and outperforms them on certain kinds of target distribution. As a result, the algorithm has become popular, especially in astronomy Vanderburg, Montet, Johnson *et al.* (2015); Crossfield, Petigura, Schlieder *et al.* (2015).

However, questions remain about the behaviour of the AIES on high dimensional problems. In Section 3 we test the method on a correlated Gaussian target distribution and discuss the observed behaviour that arises in high dimensions. Section 4 consists of a mathematical exploration of this behaviour.

2 The AIES algorithm

The AIES algorithm works by evolving a set of L samples, called *walkers*, of n parameters. A walker can be considered as a vector in n -dimensional space. At each step, the set of walkers evolves by

^{*}Department of Statistics, The University of Auckland, Private Bag 92019, Auckland 1142, New Zealand
 dhui890@aucklanduni.ac.nz, jesse.goodman@auckland.ac.nz, brendon.brewer@gmail.com

[†]To whom correspondence should be addressed

proposing a new position for one walker, and accepting this new position with a Metropolis-Hastings-type acceptance probability. The aim is to simulate the distribution specified by a target density function $\pi(\mathbf{x})$ on n -dimensional space.

Several kinds of proposals are possible, and we describe the *stretch move* used in `emcee`. Superscripts will denote walkers and subscripts will denote coordinates. Thus $\mathbf{X}^{(j)}(t)$ means the position (in n -dimensional space) of the j^{th} walker, $j = 1, \dots, L$, at time t during the algorithm, and $X_i^{(j)}(t)$ means the i^{th} coordinate of that walker, $i = 1, \dots, n$. At each step t , select a main walker $\mathbf{X} = \mathbf{X}^{(k)}(t)$. Then select a complementary walker $\mathbf{Y} = \mathbf{Y}^{(j)}(t) = \mathbf{X}^{(j)}(t)$ with $j \neq k$ chosen randomly, and define the proposal point

$$\tilde{\mathbf{X}} = Z\mathbf{X} + (1 - Z)\mathbf{Y} \quad (1)$$

where $Z = Z(t)$ is a real-valued stretching variable drawn according to the density

$$g(z) \propto \begin{cases} \frac{1}{\sqrt{z}} & \text{if } z \in [\frac{1}{a}, a] \\ 0 & \text{otherwise} \end{cases} \quad (2)$$

where a is an adjustable parameter (usually set to 2). Finally, update the walkers by replacing the main walker \mathbf{X} by the proposal point $\tilde{\mathbf{X}}$ with probability

$$p(\mathbf{X}, \mathbf{Y}, Z) = \min \left(1, Z^{n-1} \frac{\pi(\tilde{\mathbf{X}})}{\pi(\mathbf{X})} \right) = \min \left(1, Z^{n-1} \frac{\pi(Z\mathbf{X} + (1 - Z)\mathbf{Y})}{\pi(\mathbf{X})} \right) \quad (3)$$

and otherwise leaving the walkers unchanged.

In words, one can imagine the two selected walkers, \mathbf{X} and \mathbf{Y} , defining a line in parameter space. The proposal is to move the main walker \mathbf{X} to a new position along the line connecting \mathbf{X} to \mathbf{Y} . The stretching variable Z defines how far the main walker moves along this line to obtain a proposed new position, with $Z = 1$ corresponding to no change. Similar to the Metropolis-Hastings sampler, the acceptance probability depends only on the ratio of the target densities at the current and proposal points, with an additional factor Z^{n-1} arising because the proposed position is chosen from a 1-dimensional subset of n -dimensional space.

To enable parallel processing, the implementation in `emcee` performs several stretch moves simultaneously. The vector of walkers is split into two subsets $S^{(0)} = \{\mathbf{X}^{(k)} : k = 1, \dots, L/2\}$ and $S^{(1)} = \{\mathbf{X}^{(k)} : k = L/2 + 1, \dots, L\}$. In the first ‘‘half-iteration’’, all walkers in $S^{(0)}$ are simultaneously updated according to the stretch move described above, with all the complementary walkers chosen from $S^{(1)}$. In the second half-iteration, the sets are switched and all walkers in $S^{(1)}$ are simultaneously updated, with complementary walkers chosen from $S^{(0)}$. The time variable t denotes the number of iterations, each consisting of a pair of half-iterations. (Because of subtleties related to detailed balance, the main and complementary walkers must not be updated simultaneously, hence the splitting into two subsets $S^{(0)}, S^{(1)}$.)

Later, we will also consider a simpler continuous-time variant without the subsets $S^{(0)}, S^{(1)}$. In this setup, at times t chosen according to an independent exponential clock, a main walker $\mathbf{X}^{(k)}(t)$ and a complementary walker $\mathbf{X}^{(j)}(t)$ are chosen uniformly among all walkers, and a stretch move is performed. To ensure consistency of the time variable, we set the overall rate of moves to equal L , the number of walkers, so that each walker is chosen as main walker once per unit of time, on average.

The walkers collectively – i.e., the vector $\mathbf{X}(t) = (\mathbf{X}^{(1)}(t), \dots, \mathbf{X}^{(L)}(t))$ in $n \times L$ -dimensional space – form a Markov chain under either of these dynamics (either in discrete time or in continuous time, respectively). Properties of the scaling variable Z and the acceptance probability in (3) ensure that this Markov chain has an equilibrium distribution corresponding to the target density π . Specifically, the equilibrium distribution is that the walkers $\mathbf{X}^{(j)}$, $j = 1, \dots, L$, are independent random samples from the density π . Under mild conditions, this is the unique equilibrium distribution and any initial distribution will approach it as $t \rightarrow \infty$, provided that the initial points $\mathbf{X}^{(j)}(0)$ do not lie in an $(n - 1)$ -dimensional affine subspace of parameter space. (In particular, this requires that $L \geq n + 1$.) Hence, for

each sufficiently large time t , *empirical means* such as

$$\frac{1}{L} \sum_{j=1}^L f(\mathbf{X}^{(j)}(t)) \quad (4)$$

can be used as approximations of the integral $\int_{\mathbb{R}^n} f(\mathbf{x})\pi(\mathbf{x})d\mathbf{x}$, corresponding to the mean $\mathbb{E}(f(\mathbf{X}))$ when \mathbf{X} is a random variable with density function π . Similarly, empirical variances can be used to approximate $\text{Var}(f(\mathbf{X}))$. These empirical means and variances can also be averaged over different values of t . If this averaging starts after the Markov chain has burned in and spans a sufficient time compared to the mixing time, the overall estimate will improve.

As its name suggests, the AIES is invariant under affine transformations of parameter space. To explain this property, suppose \mathbf{X} has density π . Given an invertible $n \times n$ matrix \mathbf{A} and n -dimensional vector \mathbf{b} , define the affine transformation $\mathbf{x} \mapsto \mathbf{A}\mathbf{x} + \mathbf{b}$ and the random variable $\mathbf{Q} = \mathbf{A}\mathbf{x} + \mathbf{b}$. Then \mathbf{Q} has density

$$\pi'(\mathbf{q}) = \frac{\pi(\mathbf{A}^{-1}(\mathbf{q} - \mathbf{b}))}{\det \mathbf{A}}. \quad (5)$$

The fact that the proposal point in (1) is a linear combination of existing walkers causes the AIES algorithm to be invariant under affine transformations:

Proposition 1 (Affine invariance property). *Running the AIES with initial data $\mathbf{X}^{(j)}(0)$ and density π is equivalent to running the AIES with initial data $\mathbf{Q}^{(j)}(0) = \mathbf{A}\mathbf{X}^{(j)}(0) + \mathbf{b}$ and density π' .*

In particular, the AIES algorithm does not give special treatment to moves along the coordinate axes.

3 Surprising behaviour of the AIES for sampling a high dimensional Gaussian

The AIES has been used with great success in various research projects Vanderburg, Montet, Johnson *et al.* (2015); Crossfield, Petigura, Schlieder *et al.* (2015), and is especially popular in the astronomy community. However there is reason for caution if one tries to apply this method in higher dimensional problems ($n > 30$) as we will show. Unfortunately, the output from AIES may resemble the output of an MCMC algorithm initialised “in equilibrium”, yet the points obtained from the AIES might not accurately represent the target distribution.

To investigate the properties of the AIES in n dimensions we chose a correlated n -dimensional Gaussian as the target distribution. (See also the correlated Gaussian studied by Lampart (2012).)

More specifically, we used a discrete-time Ornstein-Uhlenbeck process, also known as a discrete-time auto-regressive process of the order 1, hereafter referred to as an AR(1) process. This model is well suited to be used for benchmarking, because multivariate Gaussian distributions are very common in Bayesian statistics and other applications. Besides this, the AR(1) is also useful as a prior in time series modelling.

The AR(1) distribution is the distribution of the random vector \mathbf{X} whose coordinates are defined recursively by

$$\begin{aligned} X_1 &\sim N(0, 1) \\ X_2 &\sim N(\alpha X_1, \beta^2) \\ X_3 &\sim N(\alpha X_2, \beta^2) \\ &\vdots \\ X_n &\sim N(\alpha X_{n-1}, \beta^2) \end{aligned} \quad (6)$$

where $N(\mu, \sigma^2)$ denotes a normal distribution, α is the correlation parameter, and $\beta = \sqrt{1 - \alpha^2}$. Thus \mathbf{X} has a multivariate normal distribution and the marginal distribution for each coordinate is standard

Table 1: The chosen values of the problem dimensionality n , along with the obtained mean $\hat{\mu}_n$ and standard deviation $\hat{\sigma}_n$ of the last half of the run of 1000 iterations, where the initial conditions were generated by drawing each coordinate of each walker independently from a normal $N(0, 1)$ distribution.

n	$\hat{\mu}_n$	$\hat{\sigma}_n$	mean acceptance fraction
10	0.0495	0.9688	0.419
50	0.0725	0.5481	0.192
100	-0.0063	0.3862	0.139

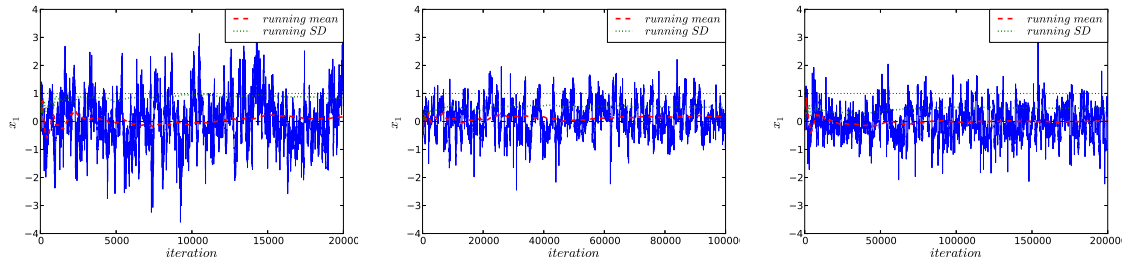
normal (mean zero, standard deviation 1), so it should be straightforward to verify whether the output of the AIES is correct. We have arbitrarily chosen the values of coordinate x_1 as a probe of the convergence properties of the AIES. Since all the coordinates have the same marginal distributions the coordinate x_1 has no particular significance over the other coordinates in this problem.

We sampled the target distribution using `emcee` Foreman-Mackey, Hogg, Lang *et al.* (2013), using a run length of 1000 iterations, $\alpha = 0.9$, number of walkers $L = 2n$, and different dimensions n displayed in Table 1. The initial conditions were generated by drawing each coordinate of each walker independently from a normal $N(0, 1)$ distribution. For a properly working MCMC method applied to this problem, the output should have an observed mean $\hat{\mu} \approx 0$ and an observed standard deviation $\hat{\sigma} \approx 1$. However, the observed values of $\hat{\sigma}$ for the obtained target distribution for $n = 50$ and $n = 100$ dimensions (displayed in Table 1) are much smaller than the true value $\sigma = 1$.

The output obtained from each run consists of a three-dimensional array with the dimensions (L , run length, n). To visualise the convergence properties this array is “flattened” to an array of length $2n(\text{run length})s$ which only contains the values of variable x_1 . The process of “flattening” reduces an two dimensional array which contains the values of coordinate x_1 of all walkers and at every iteration to an one dimensional array, therefore the final array consists of a concatenation of $X_1^{j=1..L}(t = 0)$, $X_1^{j=1..L}(t = 1)$, $X_1^{j=1..L}(t = 2)$, \dots , $X_1^{j=1..L}(t = 1000)$ in this specific order. Figure 1a displays the traceplot of the flattened array of coordinate x_1 for $n = 10$, where the dashed line displays the running average over the last 50% at point t for $0 < t < 1000$, and the dash-dotted line displays the running standard deviation over the last 50% at t for $0 < t < 1000$. The running average and running standard deviation were chosen because it removes the first 50% of the ensemble, and therefore excludes more of the output (as potential “burn-in”) over time. Figure 1a displays a short burn-in, and it seems to come to an equilibrium quite quickly. Figure 1d displays empirical values of the mean of x_1 and the variance x_1 of all walkers as a function of time, as well as the variance of q_1 to be defined in the next section. Figure 1g displays the density plot of coordinates x_1 and x_2 and it clearly shows the correlation between the two coordinates as expected. Figure 1j displays the trace plot of coordinate x_1 for several different walkers and it displays proper mixing and quick convergence. The final mean $\hat{\mu}_{n=10}$ and $\hat{\sigma}_{n=10}$ measured over the last 50% of the chain displayed in Table 1 are close to the desired values.

However, if we perform a similar analysis in higher dimensions, for example $n = 50$, the results are not as expected. Visually, the traceplot in Figure 1b seems to suggest that the burn-in period has passed, however the density plot displayed in Figure 1h shows a lack of correlation. Figure 1e shows that both the mean and the variance x_1 exhibit a sudden decrease, however it needs a large number of iterations before the variance recovers. The traceplots of the first coordinate of for different walkers displayed in Figure 1k shows poor mixing. For example, the walker for $j = 3$ remains small for most of the run, and it avoids important regions (such as the region $x_1 > 0$) that appear to have substantial probability based on Figure 1b. This is a definite undesirable property for a good MCMC method: it suggests that time scale on which walkers can vary and therefore explore parameter space is too long to give a proper representation of the target distribution. These mixing problems are reflected in the fact that the estimate $\hat{\sigma}$ is clearly too small.

For $n = 100$ the situation is even worse. The traceplot displayed in Figure 1c seems to show a successful MCMC run, although the density plot of x_1 and x_2 (Figure 1i) lacks the required correlation.

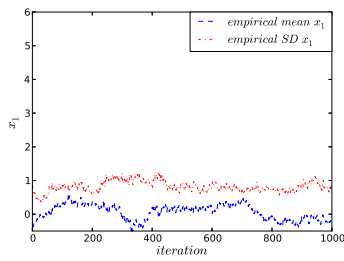


(a) $n = 10$

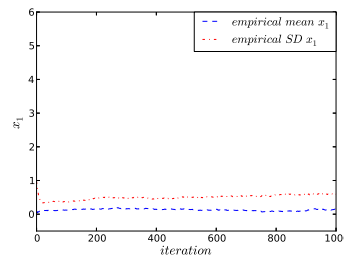
(b) $n = 50$

(c) $n = 100$

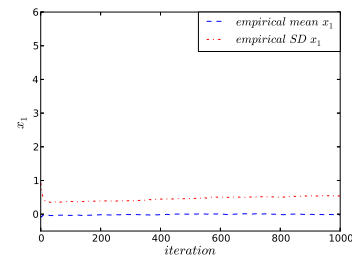
Graphs of the flattened trace plots of the first coordinate x_1 for $n = 10$, $n = 50$ and $n = 100$, and $\alpha = 0.9$, and $t = 1000$.



(d) $n = 10$

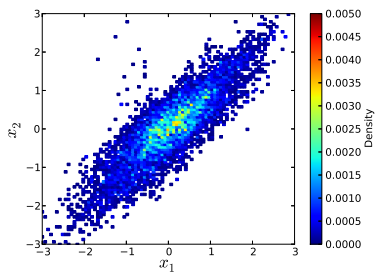


(e) $n = 50$

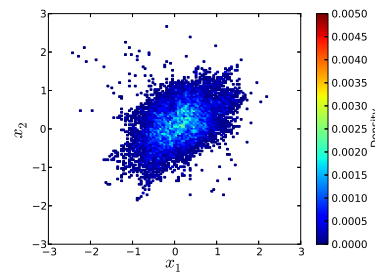


(f) $n = 100$

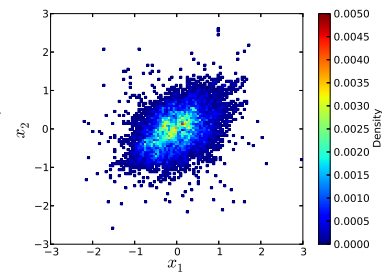
Mean values (blue) and variance (red) of x_1 over all walkers as a function of iterations t .



(g) $n = 10$

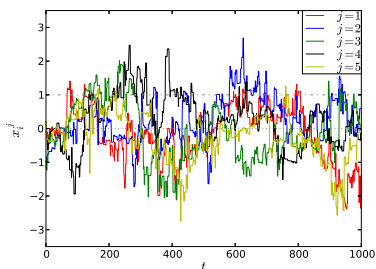


(h) $n = 50$

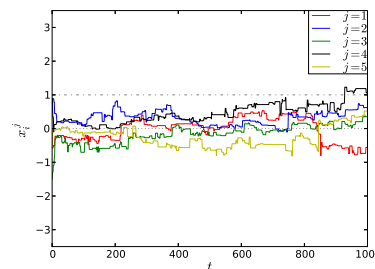


(i) $n = 100$

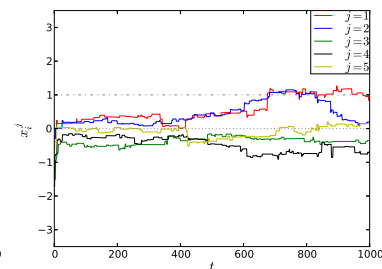
Density plot of coordinates x_1 and x_2 for all walkers from $t = 0$ to $t = 1000$



(j) $n = 10$



(k) $n = 50$



(l) $n = 100$

Trace plot of the coordinate x_1 for different walkers where $j = 1, 2, 3, 4, 5$.

Figure 1: Results of an MCMC run of an correlated Gaussian with $\alpha = 0.9$ and $t = 1000$ for different number of parameters, where $n = 10, 50, 100$.

The graphs of the mean and the variance x_1 displayed in Figure 1f show a very sudden drop for both the mean and the variance, however the recovery is extremely slow. Just like the traceplots for $n = 50$, the traceplot for $n = 100$ which can be seen in Figure 1l shows poor mixing. The estimate $\hat{\sigma}$ is also much too small.

This is our main reason why the AIES in high dimensions should be used with caution. The output can resemble a successful run while in reality, the algorithm is still going through an initial transient phase that takes a long time. Therefore the final sample does not represent the target distribution properly.

There seem to be two stages to the burn-in of AIES. There is a fast transient, which is indicated by the small scale oscillations of the dashed line, however there is a slow burn-in which is less conspicuous. As we shall explain in the next section, the fast stage reflects convergence among the “bulk” of the coordinates to be consistent with the correlation structure of the AR(1) distribution. However, the stretch moves performed during this fast stage have serious and undesirable side-effects for the ensemble of first coordinates.

4 Theoretical causes of the behaviour of the AIES for sampling a high dimensional Gaussian

The results in Section 3 suggest studying the limiting behaviour of the AIES in an appropriate limit as $n \rightarrow \infty$. This limit is somewhat complicated, not least because it requires the number of walkers to be large since $L \geq n + 1$. We begin with a description of the AIES in the limit $L \rightarrow \infty$ for fixed n and π . Then we examine a single AIES move in the limit $n \rightarrow \infty$ under a simplifying assumption. We then give a non-rigorous heuristic for the limit $n \rightarrow \infty$ that explains the behaviour described in Section 3.

4.1 The AIES with many walkers

To study the limit $L \rightarrow \infty$, it is convenient to use the continuous-time variant where the main and complementary walkers are selected uniformly among all walkers. Then the L walkers play symmetric roles and it is natural to collect them into the *empirical measure*

$$\mu^{(L)}(t) = \frac{1}{L} \sum_{j=1}^L \delta_{\mathbf{x}^{(j)}(t)}, \quad (7)$$

where $\delta_{\mathbf{x}}$ denotes the measure placing unit mass at $\mathbf{X} \in \mathbb{R}^n$. In words, the measure $\mu^{(L)}(t)$ encodes the distribution of a uniformly chosen walker at time t . Because of the assumption that both walkers X and Y are selected uniformly, it follows that $\mu^{(L)}(t)$ is itself a Markov chain.

Proposition 2. *Choose the initial walkers independently according to the distribution μ_0 . Then, in the limit $L \rightarrow \infty$, the empirical measure process $\mu^{(L)}(t)$ converges in distribution to a deterministic path μ_t with initial value μ_0 and*

$$\frac{d}{dt} \int f(\mathbf{x}) d\mu_t(\mathbf{x}) = \iint_{\mathbb{R}^n \times \mathbb{R}^n} \mathbb{E} \left(f(Z\mathbf{x} + (1-Z)\mathbf{y}) - f(\mathbf{x}) \right) p(\mathbf{x}, \mathbf{y}, \mathbf{z}) d\mu_t(\mathbf{x}) d\mu_t(\mathbf{y}). \quad (8)$$

To interpret this result, suppose \mathbf{X} and \mathbf{Y} are independent samples distributed according to the current empirical measure μ_t . Choose Z according to the density in (2) and define $\tilde{\mathbf{X}} = \mathbf{X}Z + \mathbf{Y}(1-Z)$, as in (1). Set \mathbf{X}' to be $\tilde{\mathbf{X}}$ with probability $p(\mathbf{X}, \mathbf{Y}, Z)$ and \mathbf{X} otherwise, and let μ'_t denote the measure encoding the distribution of \mathbf{X}' , averaged over all the possibilities for \mathbf{X} , \mathbf{Y} and Z . Then Proposition 2 says that the measure μ_t evolves by travelling in the direction of the line (in the space of measures) joining μ_t to μ'_t .

The intuition behind Proposition 2 is that the average effect of each move is to take μ_t in the direction toward μ'_t . Each move changes a fraction $1/L$ of the measure $\mu^{(L)}(t)$, but this is offset by the fact that

moves occur at rate L . The fact that the limiting dynamics are deterministic is established by examining products of empirical means.

The authors did not find any explicit solutions to the system of equations (8). (In the simplest case $n = 1$, $\pi(\mathbf{x}) \propto \exp(-\mathbf{x}^2/2)$, i.e., a one-dimensional standard normal density, any normal initial data that is not standard becomes non-normally distributed at positive times and does not appear to follow any simple trajectory.) However, it is possible to consider (8) for other choices for the function p . The simplest possible choice is to take $p = 1$, i.e., to accept proposals unconditionally. Even in this case, we still cannot solve (8), but we can make the following observation.

Proposition 3. *Consider the system of equations (8) where the function $p(\mathbf{x}, \mathbf{y}, z)$ is replaced by the constant 1. If the i^{th} coordinate has finite second moment under the initial measure, $\int x_i^2 d\mu_0(\mathbf{x}) < \infty$, then its mean $\int x_i d\mu_t(\mathbf{x})$ is constant and its variance $\text{Var}_{\mu_t}(x_i) = \int x_i^2 d\mu_t(\mathbf{x}) - (\int x_i d\mu_t(\mathbf{x}))^2$ evolves according to*

$$\frac{d}{dt} \text{Var}_{\mu_t}(x_i) = \mathbb{E}(Z(Z-1)) \text{Var}_{\mu_t}(x_i). \quad (9)$$

Thus the variance will either grow or decay exponentially, depending on whether $\mathbb{E}(Z(Z-1))$ is positive or negative.

4.2 The AIES for a high-dimensional standard Gaussian

We next consider a single stretch move for the target density

$$\pi'(\mathbf{x}) = c \cdot \exp\left(-\frac{1}{2} \sum_{i=1}^n x_i^2\right) \quad (10)$$

corresponding to an n -dimensional standard normal distribution. The acceptance probability from (3) becomes $p(\mathbf{x}, \mathbf{y}, z) = \min\{1, \exp(h(\mathbf{x}, \mathbf{y}, z))\}$ where

$$h(\mathbf{x}, \mathbf{y}, z) = (n-1) \log z - \frac{1}{2} \sum_{i=1}^n (zx_i + (1-z)y_i)^2 + \frac{1}{2} \sum_{i=1}^n x_i^2. \quad (11)$$

To analyze $h(\mathbf{x}, \mathbf{y}, z)$, we make the following assumption about the randomly chosen walkers \mathbf{X} and \mathbf{Y} for the move under consideration.

Assumption 4. *The coordinates of X_1, \dots, X_n and Y_1, \dots, Y_n are mutually independent and identically distributed (i.i.d.) with common mean μ and common variance σ^2 .*

Proposition 5. *Subject to Assumption 4, $\frac{1}{n}h(\mathbf{X}, \mathbf{Y}, z) \rightarrow f_\sigma(z)$ where*

$$f_\sigma(z) = \log z - \sigma^2 z(z-1). \quad (12)$$

The acceptance probability $p(\mathbf{X}, \mathbf{Y}, z)$ converges to 1 if $f_\sigma(z) > 0$ and to 0 if $f_\sigma(z) < 0$.

Proof. This is an application of the Law of Large Numbers:

$$\begin{aligned} \frac{h(\mathbf{x}, \mathbf{y}, z)}{n} &= -\frac{\log z}{n} + \frac{1}{n} \sum_{i=1}^n \left(\log z - \frac{1}{2}(z^2-1)x_i^2 - z(1-z)x_i y_i - \frac{1}{2}(1-z)^2 y_i^2 \right) \\ &\rightarrow 0 + \mathbb{E} \left(\log z - \frac{1}{2}(z^2-1)x_i^2 - z(1-z)x_i y_i - \frac{1}{2}(1-z)^2 y_i^2 \right) \\ &= \log z - \frac{1}{2}(z^2-1)(\sigma^2 + \mu^2) - z(1-z)\mu \cdot \mu - \frac{1}{2}(1-z)^2(\sigma^2 + \mu^2) \\ &= \log z - \sigma^2 \frac{z^2-1+(1-z)^2}{2} - \mu^2 \frac{z^2-1+2z(1-z)+(1-z)^2}{2} \\ &= f_\sigma(z). \end{aligned} \quad (13)$$

The convergence of $p(\mathbf{X}, \mathbf{Y}, z) = \min(1, \exp(h(\mathbf{X}, \mathbf{Y}, z)))$ follows because either $h(\mathbf{X}, \mathbf{Y}, z) \rightarrow \infty$ or $h(\mathbf{X}, \mathbf{Y}, z) \rightarrow -\infty$ depending on the sign of $f_\sigma(z)$. \square

The behaviour of $f_\sigma(z)$ for three values of σ is shown in Figure 2. When $\sigma > 1$, $f_\sigma(z)$ is positive for z slightly smaller than 1. When $\sigma < 1$, $f_\sigma(z)$ is positive for z slightly larger than 1. In the critical case $\sigma = 1$, $f_\sigma(z)$ is always negative and a Taylor expansion gives

$$f_1(z) \approx -\frac{3}{2}(z-1)^2 \quad \text{for } z \text{ close to } 1. \quad (14)$$

The interpretation of Assumption 4 and Proposition 5 is as follows. Freeze the AIES algorithm at time t . The walkers \mathbf{X} and \mathbf{Y} to be used in the next move will be drawn independently from the current population of walkers. Assume without proof that the coordinates X_1, \dots, X_n and Y_1, \dots, Y_n are i.i.d. (or at least are sufficiently close to i.i.d. for the conclusion of Proposition 5 to hold). Then the acceptance probability at the next move is effectively independent of the actual walkers \mathbf{X} and \mathbf{Y} . Furthermore the dependence on z is determined only by the variance σ^2 .

To illustrate this effect, we ran three different MCMC-runs on an uncorrelated Gaussian for about 1000 times of 1 iteration. Each of these 1000 iterations was started with a re-initialized initial condition, where each of the n components of every of L walkers are drawn from a Gaussian distribution $N(0, \sigma^2)$ with $\sigma^2 \in \{0.1, 1, 2\}$. We obtained the accepted z -values, and created histograms displayed in Figure 3. For $\sigma \neq 1$, a sharp cut-off is observed across the value $Z = 1$, becoming more pronounced as n increases. Values of z on the predicted side of 1 are accepted almost unconditionally. For $\sigma = 1$, the approximation $p(\mathbf{X}, \mathbf{Y}, z) \approx \exp(-cn(z-1)^2)$ suggests that the accepted values of Z will be roughly normally distributed with a spread that decreases with n , and this prediction is reflected in the histograms.

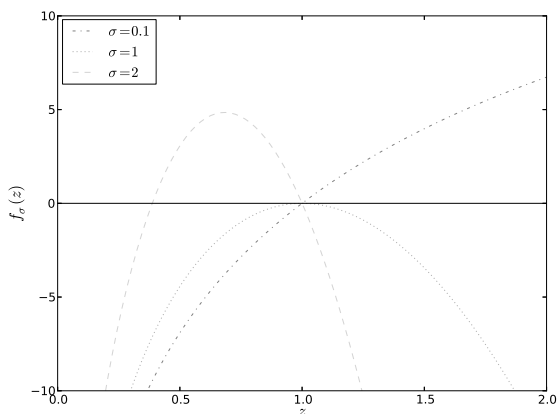


Figure 2: The graph of the function $F(z) = n(\log z - \sigma^2(t)z(z-1))$ as a function of z for $\sigma(t) = 0.1$ (dashed-dotted line), $\sigma(t) = 1$ (dotted line), and $\sigma(t) = 2$ (dashed line).

4.3 The AIES for a high-dimensional correlated Gaussian

We now turn to the correlated AR(1) model from Section 3. Based on the analysis of Sections 4.1 and 4.2, we present a heuristic that explains the behaviour observed in Section 3.

Because of Proposition 1, we can apply an affine transformation to this correlated Gaussian distribution into an uncorrelated one. Recalling (6), the relevant transformation $\psi(x)$ will be

$$\begin{aligned} q_1 &= \psi_1(x) = x_1, & x_1 &= q_1, \\ q_i &= \psi_i(x) = \frac{x_i - \alpha x_{i-1}}{\beta}, & x_i &= \alpha x_{i-1} + \beta q_i, \quad i \geq 2. \end{aligned} \quad (15)$$

A random variable \mathbf{X} has the AR(1) distribution if and only if the corresponding \mathbf{Q} has the n -dimensional standard normal distribution. This problem therefore falls in the setup of Section 4.2 with density π' when expressed in terms of the \mathbf{q} -coordinate system.

Note that the coordinate q_1 plays a distinguished role, directly measuring the quantity of interest from the original system. (Different transformations can be used to emphasise other quantities from the original system.) The coordinates q_2, \dots, q_n can be thought of as encoding how closely the coordinates x_i conform to the correlation structure of the AR(1) distribution.

We will analyse the AIES algorithm from the perspective of the \mathbf{q} -coordinate system. To begin, we must specify the initial walker coordinates. In practice, we are unlikely to have any knowledge of the \mathbf{q} -coordinate system. Therefore the most obvious choice is to generate i.i.d. initial coordinates $X_i^{(j)}(0)$

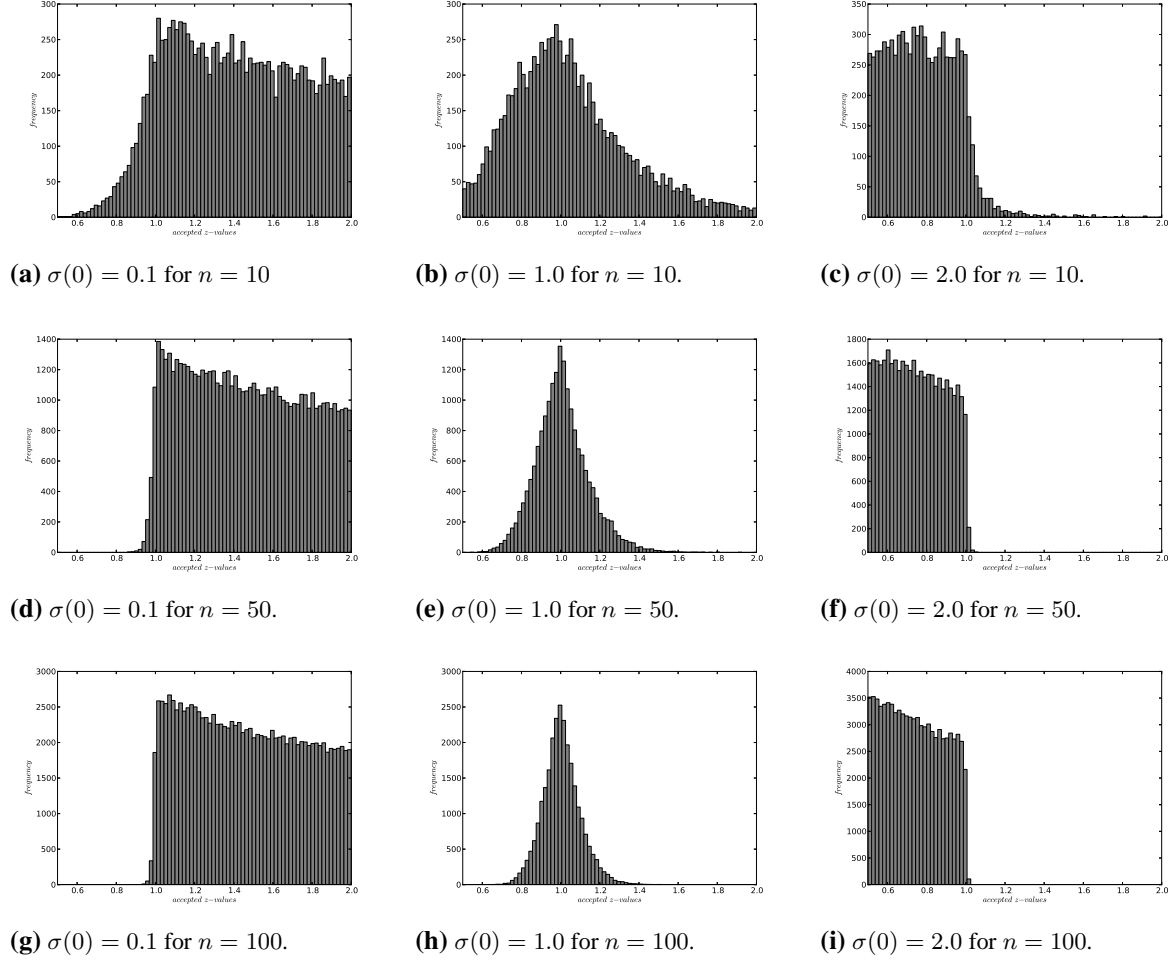


Figure 3: Histogram of the accepted z for $n = 10, 50, 100$ and $\sigma(0) = 0.1, 1, 2$ for an MCMC run of an uncorrelated Gaussian with $t = 1000$.

in the \mathbf{x} -coordinate system. By (15), the initial \mathbf{q} -coordinates have variances

$$\begin{aligned} \text{Var}(Q_1^{(j)}(0)) &= \text{Var}(\psi_1(\mathbf{X}^{(j)}(0))) = \text{Var}(X_1^{(j)}(0)), \\ \text{Var}(Q_i^{(j)}(0)) &= \text{Var}(\psi_i(\mathbf{X}^{(j)}(0))) = \frac{1 + \alpha^2}{\beta^2} \text{Var}(X_i^{(j)}(0)), \quad i \geq 2. \end{aligned} \tag{16}$$

Note that the variance for $i \geq 2$ is larger by a factor $\frac{1 + \alpha^2}{1 - \alpha^2}$ compared to $i = 1$. This factor becomes large in the highly correlated case where α is close to 1.

To proceed with our heuristic analysis, we introduce without proof the following assumption.

Assumption 6. *At every time t in the AIES algorithm, the \mathbf{q} -coordinates $(Q_i^{(j)}(t), i = 1, \dots, n)$ (possibly excluding the first coordinate) of a randomly chosen walker are i.i.d. with common mean $\mu(t)$ and common variance $\sigma(t)^2$ – or at least are sufficiently close to i.i.d. that the conclusions of Proposition 5 apply.*

In reality, the assumption of independence will not hold even at time $t = 0$; the initial \mathbf{q} -coordinates are only weakly correlated in the sense that $\text{Cov}(Q_i^{(j)}(0), Q_{i'}^{(j)}(0)) = 0$ if $|i - i'| \geq 2$. Even if the initial q -coordinates were chosen in an i.i.d. way, there would be no reason for the AIES dynamics to preserve this property at later times. However, Proposition 5 depends only on a Law of Large Numbers effect, and at the level of a heuristic it is reasonable to expect this effect to be robust.

Subject to Assumption 6, Proposition 5 asserts that the acceptance probability $p(\mathbf{X}, \mathbf{Y}, Z)$ is essentially independent of the actual walker positions \mathbf{X} and \mathbf{Y} . In particular, it is essentially independent of

the actual first q -coordinates $\psi_1(\mathbf{X})$ and $\psi_1(\mathbf{Y})$. From the perspective of the first coordinates only, the AIES dynamics are approximated¹ by the following:

1. Select walkers \mathbf{X} and \mathbf{Y} , stretching variable Z , and proposal $\tilde{\mathbf{X}} = Z\mathbf{X} + (1 - Z)\mathbf{Y}$ as usual. Write $\mathbf{Q} = \psi(\mathbf{X})$, $\mathbf{U} = \psi(\mathbf{Y})$, and $\tilde{\mathbf{Q}} = \psi(\tilde{\mathbf{X}})$.
2. Define the modified acceptance probability

$$p' = \min \left(1, Z^{n-1} \exp \left(-\frac{1}{2} \sum_{i=2}^n \left((ZQ_i + (1 - Z)U_i)^2 - Q_i^2 \right) \right) \right) \quad (17)$$

solely in terms of \mathbf{q} -coordinates 2 to n . In coordinates 2 to n , update from \mathbf{Q} to $\tilde{\mathbf{Q}}$ with probability p' .

3. For each move accepted in step 2, apply the same move to the first coordinate with probability 1.

From the perspective of the first coordinates, the accepted stretching variables Z follow a modified distribution $\tilde{Z}(t)$ that may vary over time as the other q -coordinates equilibrate. Stretching variables $\tilde{Z}(t)$ also arrive at a reduced average frequency $r(t) = \mathbb{E}(p')$. However, when they arrive, they are always accepted, as in Proposition 3. We therefore make the following predictions:

Prediction 7. *Write*

$$\text{Var}_t(X_1) = \frac{1}{L} \sum_{j=1}^L X_1^{(j)}(t)^2 - \left(\frac{1}{L} \sum_{j=1}^L X_1^{(j)}(t) \right)^2 \quad (18)$$

for the empirical variance of X_1 as determined by the walkers at time t . Then:

- When $\sigma(t) \gg 1$, $\text{Var}_t(X_1)$ will decrease rapidly, regardless of whether it is too large or too small compared to the true value 1.
- When $\sigma(t) \ll 1$, $\text{Var}_t(X_1)$ will increase rapidly, regardless of whether it is too large or too small compared to the true value 1.
- When $\sigma(t)$ is close to 1, $\text{Var}_t(X_1)$ will not converge quickly to the true value 1.
- Quantitatively,

$$\frac{d}{dt} \text{Var}_t(X_1) \approx r(t) \mathbb{E} \left(\tilde{Z}(t)(\tilde{Z}(t) - 1) \right) \text{Var}_t(X_1). \quad (19)$$

To test Prediction 7, we graphed the average empirical standard deviation of all \mathbf{q} -coordinates at times close to the fast burn-in phase: see Figure 4. The initial value is greater than 1, as predicted by (16), and has equilibrated around 1 after about 10 iterations. In Figure 5, the empirical variance $\text{Var}_t(X_1)$ of all first coordinates is graphed over the same time interval. Especially for $n = 50$ and $n = 100$, the variance decreases rapidly at first, then levels off around the same time, 10 iterations. This confirms the qualitative parts of Prediction 7.

We also tested the quantitative prediction in equation (19). At five selected times $t = 2, 8, 14, 30, 50$, we overlaid the predicted tangent line from Prediction 7 – i.e., the line with slope given by the right-hand side of equation (19) – onto the graph of $\text{Var}_t(X_1)$. The quantities $r(t)$ and $\mathbb{E} \left(\tilde{Z}(t)(\tilde{Z}(t) - 1) \right)$ in equation (19) depend on the hypothetical distribution of all Z values that would be accepted given the actual walkers at time t , and were therefore approximated by observing the accepted Z values from 100 auxiliary emcee iterations, each initialised with the actual walker positions at time t .

The results are shown in Figure 5. For $n = 10$, the predicted lines do not very closely track the underlying curve, but for $n = 50$ and $n = 100$ there is good agreement with Prediction 7.

¹A careful justification of this approximation involves more than the fact that $p(\mathbf{X}, \mathbf{Y}, z)$ is largely independent of \mathbf{X} and \mathbf{Y} . Specifically, the justification is that the probabilities $p(\mathbf{X}, \mathbf{Y}, Z)$ and p' are unlikely to have a large difference. This holds because according to Proposition 5 the quantity $h(\mathbf{X}, \mathbf{Y}, Z)$ is likely to be either large and positive (in which case it is unlikely to become negative after removing the $i = 1$ term, so that both p and p' will be 1) or large and negative (in which case removing the $i = 1$ term may make a difference, but both p and p' will still be small). This reasoning will break down when $h(\mathbf{X}, \mathbf{Y}, Z)$ has the possibility to be small, which will happen when Z and $\sigma(t)$ are close to 1.

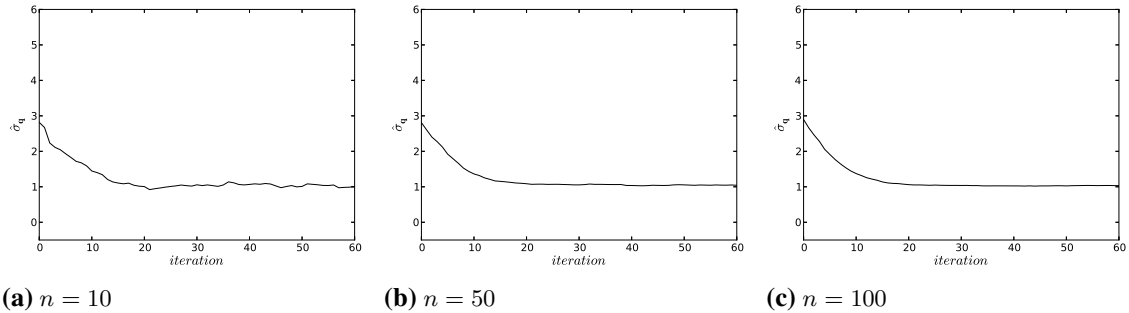


Figure 4: The variance of q over all walkers and coordinates for $\alpha = 0.9$, $t = 1000$

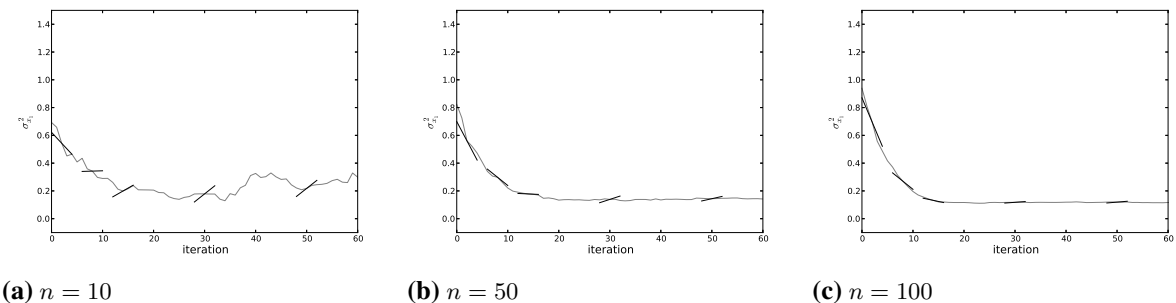


Figure 5: In grey: the empirical variance $\text{Var}_t(X_1)$, as estimated by the first coordinates $X_1^{(j)}(t)$ of all walkers at time t , for $0 \leq t \leq 60$. Overlaid in black: five predicted “tangent” lines for the curve, at times $t = 2, 8, 14, 30, 50$, based on the slopes predicted in Equation (19).

5 Discussion

Even though the AEIS has been used with success in the past on numerous occasions, we advise caution in high dimensional problems. The benchmark model we used to probe the problems of the AEIS was a relatively simple model which already fails at $n = 50$, and we expect problems to be even worse for more strongly correlated, or more complex, models.

Unsurprisingly, other MCMC methods work more efficiently for the benchmark model we chose. For instance, if the target distribution is interpreted as a posterior distribution with an uncorrelated Gaussian as the prior, then the elliptical slice sampler of Murray, Adams & MacKay (2010) gives good results. If the target distribution is interpreted as a time-discretisation of a continuous process (in this case the Ornstein-Uhlenbeck process U_t , the centred Gaussian process with $\text{Cov}(U_t, U_s) = e^{-|t-s|}$, over the time interval $[0, \alpha n]$) then the ideas of Cotter, Roberts, Stuart *et al.* (2013) can be used to obtain an MCMC method that handles dimensionality well. However, these alternative methods require additional structure and analysis of the model. Especially if the model is more complicated, the possibility of slow convergence may be a reasonable price to pay for the simplicity and generality of the AIES; the difficulty here is that the slow convergence can be hard to detect.

Indeed, an important issue in practice is how to know whether the AIES is experiencing the kind of problems we describe. Evidently, it is not possible to rely on knowing the true target distribution, as we did. One common diagnostic is to report the acceptance ratio (the fraction of proposal steps actually accepted). If the ratio is too low, the MCMC algorithm is not exploring quickly; if it is too high, the algorithm is accepting too many moves without regard to the actual density and may not have finished exploring. In our model, the acceptance ratio did not indicate any problem (see the values in Table 1). By contrast, our analysis shows that the *profile* of accepted Z values – particularly if they clustered on either side of $z = 1$ – gave relevant information about the system.

Another possibility is to use automated convergence criteria. Unfortunately, checking the perfor-

mance of such criteria was outside of the scope of this research. However, a good follow up would be to investigate how successfully well-known convergence criteria can detect this behaviour.

Finally, traceplots are common tools to visually assess the performance of MCMC methods. Because the AIES is an ensemble method, some adaptations are necessary. For instance, the straightforward traceplots in Figure 1a, 1b and 1c, showing the first coordinates over all walkers and steps, give an impression of the range of likely values but give little insight into the different mixing properties. Instead, selecting a small number of walkers, as in Figures 1j, 1k and 1l, shows that individual walkers are mixing well (relative to the range of likely values) when $n = 10$, but not when $n = 50$ or $n = 100$. In Figure 1j for $n = 10$, it seems like the first coordinate of each walker is free to explore parameter space (between about -2 and 2 , a region where most walkers appear to spend most of their time, according to Figure 1a). By contrast, in Figures 1k and 1l for $n = 50$ and $n = 100$, the first coordinates of each walker seem to be confined to much narrower regions (even accounting for unduly restricted range of walker positions in Figures 1b and 1c) and the relative order among the sampled walkers changes much less frequently. In our examination of the AIES in this high-dimensional model, this was the only sign of slow convergence that we could identify without knowing the characteristics of the true target distribution.

In summary, high dimensions can bring problems that make the AIES converge slowly and, more disturbingly, appear to have converged even when it has not. Knowing the structure of the true distribution allowed us to make accurate predictions about the evolution of the AIES for our chosen model. Looking at two measures arising from the algorithm – the profile of accepted Z values and a subsample traceplot of a few walkers – gave a possible signal of slow convergence. Such diagnostics, and a measure of caution, should be used when applying the AIES to high-dimensional problems.

References

- COTTER, S.L., ROBERTS, G.O., STUART, A.M. & WHITE, D. (2013). MCMC methods for functions: Modifying old algorithms to make them faster. *Stat. Sci.* **28**, 424–446. doi:10.1214/13-STS421.
- CROSSFIELD, I.J.M., PETIGURA, E., SCHLIEDER, J.E., HOWARD, A.W., FULTON, B.J., ALLER, K.M., CIARDI, D.R., LÉPINE, S., BARCLAY, T., DE PATER, I., DE KLEER, K., QUINTANA, E.V., CHRISTIANSEN, J.L., SCHLAFLY, E., KALTENEGGER, L., CREPP, J.R., HENNING, T., OBERMEIER, C., DEACON, N., WEISS, L.M., ISAACSON, H.T., HANSEN, B.M.S., LIU, M.C., GREENE, T., HOWELL, S.B., BARMAN, T. & MORDASINI, C. (2015). A nearby M star with three transiting super-Earths discovered by K2. *Astrophys. J.* **804**, 10. doi:10.1088/0004-637X/804/1/10.
- FOREMAN-MACKEY, D., HOGG, D.W., LANG, D. & GOODMAN, J. (2013). Emcee: The MCMC hammer. *Publ. Astron. Soc. Pac.* **125**, 306–312.
- GEMAN, S. & GEMAN, D. (1984). Stochastic relaxation, Gibbs distributions, and the Bayesian restoration of images. *IEEE Trans. Pattern Anal. Mach. Intell.* **6**, 721–741. doi:10.1109/TPAMI.1984.4767596.
- GOODMAN, J. & WEARE, J. (2009). Ensemble samplers with affine invariance. *Commun. Appl. Math. Comput. Sci.* **5**, 65–80.
- HASTINGS, W.K. (1970). Monte Carlo sampling methods using Markov chains and their applications. *Biometrika* **57**, 97–109.
- LAMPART, T. (2012). Implementation and performance comparison of an ensemble sampler with affine invariance. *Technical report*, MOSAIC group, Institute of Theoretical Computer Science, Department of Computer Science, ETH Zürich.
- METROPOLIS, N., ROSENBLUTH, A.W., ROSENBLUTH, M.N., TELLER, A.H. & TELLER, E. (1953). Equation of state calculations by fast computing machines. *J. Chem. Phys.* **21**, 1087–1092.
- MURRAY, I., ADAMS, R.P. & MACKAY, D.J. (2010). Elliptical slice sampling. *J. Mach. Learn. Res. Workshop Conf. Proc.* **9**, 541–548.
- NEAL, R.M. (2003). Slice sampling. *Ann. Stat.* **31**, 705–741.
- NEAL, R.M. (2011). MCMC using Hamiltonian dynamics. In *Handbook of Markov Chain Monte Carlo*, chap. 5. Chapman & Hall/CRC, pp. 113–162. See also arXiv:1206.1901 [stat.CO].
- VANDEBURG, A., MONTET, B.T., JOHNSON, J.A., BUCHHAVE, L.A., ZENG, L., PEPE, F., CAMERON, A.C., LATHAM, D.W., MOLINARI, E., UDRY, S., LOVIS, C., MATTHEWS, J.M., CAMERON, C., LAW, N., BOWLER, B.P., ANGUS, R., BARANEC, C., BIERYLA, A., BOSCHIN, W., CHARBONNEAU, D., COSENTINO, R., DUMUSQUE, X., FIGUEIRA, P., GUENTHER, D.B., HARUTYUNYAN, A., HELLIER, C., KUSCHNIG, R., LOPEZ-MORALES, M., MAYOR, M., MICELA, G., MOFFAT, A.F.J., PEDANI, M., PHILLIPS, D.F., PIOTTO, G., POLLACCO, D., QUELOZ, D., RICE, K., RIDDLE, R., ROWE, J.F., RUCINSKI, S.M., SASSELOV, D., SÉGRANSAN, D., SOZZETTI, A., SZENTGYORGYI, A., WATSON, C. & WEISS, W.W. (2015). Characterizing K2 planet discoveries: A super-Earth transiting the bright K dwarf HIP 116454. *Astrophys. J.* **800**, 59 pages.